Article

Optimal Thickness of Double-Layer Graphene-Polymer Absorber for 5G High-Frequency Bands

Alessandro Giuseppe D'Aloia [1,2,]*, Marcello D'Amore [1,2] and Maria Sabrina Sarto [1,2]

[1] Department of Astronautical, Electrical and Energy Engineering, Sapienza University of Rome, 00184 Rome, Italy
[2] Research Center on Nanotechnology Applied to Engineering of Sapienza (CNIS), Sapienza University of Rome, Via Eudossiana 18, 00184 Rome, Italy
[*] Correspondence: alessandrogiuseppe.daloia@uniroma1.it; Tel.: +39-0644-585-806

Abstract: A new analytical approach to optimize the thicknesses of a two-layer absorbing structure constituted by a graphene-based composite and a polymer dielectric spacer backed by a metallic layer acting as perfect electric conductor (PEC) is proposed. The lossy sheet is made by an epoxy-based vinyl ester resin filled with graphene nanoplatelets (GNPs) characterized by known frequency spectra of the complex permittivity. The optimal thicknesses are computed at the target frequencies of 26, 28, and 39 GHz in order to obtain a −10 dB bandwidth able to cover the 5G frequency bands between 23.8 and 40 GHz. The resulting absorbing structures, having a total thickness lower than 1 mm, are excited by transverse magnetic (TM) or electric (TE) polarized plane waves and the absorption performances are computed in the 5G high frequency range.

Keywords: two-layers absorber; graphene-based composite; oblique incidence; 5G absorption performances

1. Introduction

Over the next decade, the fifth generation of wireless technology, indicated as 5G, will play a key-role in forthcoming telecommunications and mobile networks, allowing for the development of smart integrated networks capable of revolutionizing our daily lives [1]. For instance, the data transmission speed will rise sharply, up to 100 times the speed of current wireless data transmission [2], and the latency, i.e., the time it takes to send data from one device to the next via wireless network, will drop drastically, reaching values as low as 1 ms [3].

Such a revolution requires the allocation of new frequency bands, from some gigahertz up to nearly one hundred gigahertz [3]. As a drawback, the risk of unexpected electromagnetic (EM) interference (EMI) increases. Hence, EMI issues must be taken seriously into account and the use of EM absorbers is a promising EMI countermeasure [4].

The design and realization of new absorbers is becoming crucial and large efforts have been made in the development of new high-performance absorbing materials and screens. In fact, new absorbers should conjugate high EM performances with other characteristics, such as lightness, simple structure, flexibility, resistance to corrosion, and cost effectiveness [4–6].

One of the most investigated absorbing panels is the dielectric Salisbury screen, consisting of a lossy layer followed by a PEC-backed dielectric spacer. However, the main limitation is represented by the thickness that, for frequency applications from a few up to 40 GHz, is in the range of centimeters [7]. In this regard, the use of custom-tailored graphene-based composites as lossy layers allows to overcome this bottleneck. Therefore, two-layers absorbing structures are attracting ever-growing interest and the optimal design of microwave absorbers consisting of a graphene-based custom tailored composite material and a PEC-backed dielectric spacer is nowadays of primary interest. In particular, the selection of EM properties and thicknesses of both layers are key factors for the realization of high-performing absorbing screens with absorption coefficients lower than −10 dB in

a wide frequency band within the 5G spectrum allocations. Thus, the design process is attracting growing interest among scientists and technicians, and efficient simulation tools are urgently needed in order to optimize the EM project of absorbers operating also in the 5G spectrum.

Nowadays, the optimum thicknesses and the EM properties of the layers constituting the absorber structures are estimated using genetic algorithms or linear regression analysis techniques [8–11]. However, these methods need complex numerical procedures, often based on simplifying hypotheses. Furthermore, the resulting absorbing structures can be of difficult realization, compromising the cost-effectiveness and the absorber simplicity.

More simple approaches are focused on the preliminary EM investigation of the lossy layer, which should be characterized by an intrinsic impedance close to the free-space one. Moreover, quite often the optimal thicknesses are selected using tentative numerical methods [12–15] or explicit analytical expressions based on simplifying hypotheses [16–19].

This paper proposes a new analytical approach to optimize the thicknesses of the layers constituting a two-layers absorbing structure. This approach is tested on an absorbing structure consisting of a graphene-based composite and a polymer dielectric layer acting as lossy sheet and spacer, respectively.

In particular, the considered lossy sheet is made of an epoxy-based vinyl ester resin filled with different amounts of graphene nanoplatelets (GNPs), i.e., small stacks of graphene layers having lateral dimensions in micrometer range and thicknesses ranging between 2 nm and 10 nm [15].

GNPs have gained most attention as graphene based nanofillers in polymer composites since they are extremely cheap, easily processable, and characterized by outstanding mechanical properties, along with high thermal and electrical conductivities [16]. Furthermore, they are suitable for large scale production [20] and represent an excellent alternative to the use of pure graphene, which is not yet produced on a large scale and its price is still high [20–22]. The current and future applications of GNPs filled composites are unlimited, from materials with enhanced mechanical and thermal behavior up to new functional materials or conductive coatings, such as sensors, new electronic devices, energy harvesting, and EM shields [6,15,20–23]. Moreover, they allow the production of innovative materials with outstanding electromagnetic properties, suitable for the realization of next generation microwave absorbers [24–26]. Hence, GNPs filled composites are considered in this study. In particular, the new design process is applied to evaluate the optimum configuration of the selected two-layers absorbing structure in the 5G high frequency range up to 40 GHz and to compute absorption performances considering graphene based lossy layers employing different amounts of GNPs.

2. Structure of the Graphene-Polymer Absorber

The considered Salisbury screen structure is composed of a graphene-based lossy sheet and a polymer dielectric spacer, followed by a metallic layer acting as a perfect electric conductor (PEC). The polymer spacer and the composite are indicated in Figure 1 as layer 1 and layer 2, respectively.

The absorber is illuminated by a transverse magnetic (TM) or transverse electric (TE) polarized plane wave with incidence angle θ_0, as shown in Figure 1. The absorber is supposed to be of infinite dimensions along the y- and z- axes.

The spacer layer is made of polypropylene (PP), having relative permittivity $\varepsilon_1 = 2.36$, assumed constant in the considered frequency bandwidth, and relative permeability $\mu_1 = 1$.

The graphene-based lossy sheet, which does not show any magnetic property (hence $\mu_2 = 1$), is constituted by an epoxy-based vinyl ester resin filled with different amounts of GNPs.

The relative permittivity $\varepsilon_2 = \varepsilon_2' - j\varepsilon_2''$ of the resulting GNP composites has been experimentally measured, modelled, and predicted by means of an analytical procedure based on the Maxwell Garnet formula [15,26].
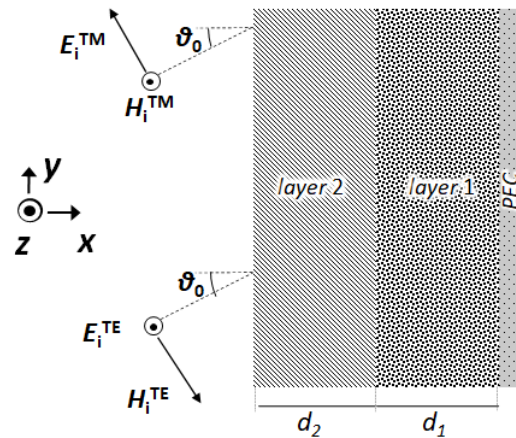
Figure 1. Absorber structure consisting of a PEC-backed polymer dielectric spacer (layer 1) and a graphene-based lossy sheet (layer 2). $E_i^{TM(TE)}$ and $H_i^{TM(TE)}$ are the incident electric and magnetic fields in case of TM or TE polarizations.

The real and imaginary parts, ε_2' and ε_2'', of the permittivity are represented in Figure 2a,b, respectively, for composites filled with a GNP weight concentration ranging between 0.25% and 4%.
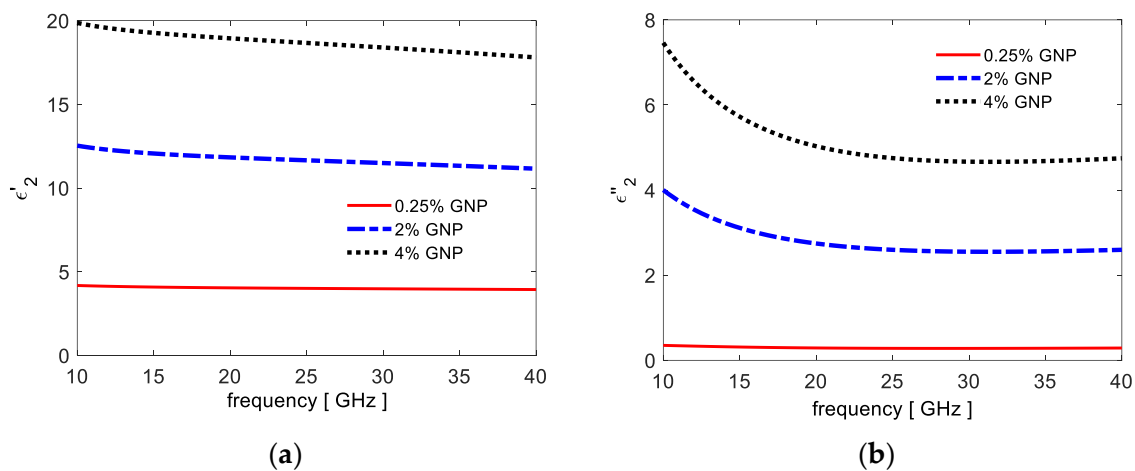

(**a**)

(**b**)

Figure 2. Frequency spectra of the real (**a**) and imaginary (**b**) parts of the permittivity of the graphene based composite employing different amounts of GNPs.

3. Optimal Absorber Design

The reflection coefficient in case of TM(TE) polarization, $R^{TM(TE)}$, is evaluated as:

$$R^{TM(TE)} = \left| \frac{Z_{in}^{TM(TE)} - \eta_0^{TM(TE)}}{Z_{in}^{TM(TE)} + \eta_0^{TM(TE)}} \right| \tag{1}$$

in which η_0^{TM} and η_0^{TE} are the TM and TE wave impedances, given by:

$$\eta_0^{TM} = \eta_0 \cos\vartheta_0 \tag{2}$$

$$\eta_0^{TE} = \frac{\eta_0}{\cos\vartheta_0} \tag{3}$$

being η_0 the free space wave impedance [25].

The TM(TE) absorber input impedance $Z_{in}^{TM(TE)}$ is computed as:

$$Z_{in}^{TM(TE)} = \eta_2^{TM(TE)} \frac{Z_{in1}^{TM(TE)} + \eta_2^{TM(TE)} \tanh(\gamma_2 d_2)}{\eta_2^{TM(TE)} + Z_{in1}^{TM(TE)} \tanh(\gamma_2 d_2)} \tag{4}$$

where $Z_{in1}^{TM(TE)}$ is the TM(TE) input impedance of the dielectric spacer layer:

$$Z_{in1}^{TM(TE)} = \eta_1^{TM(TE)} \tanh(\gamma_1 d_1) \tag{5}$$

The TM and TE wave impedances of the *i*-th layer, with *i* equal to 1 or 2, are computed as:

$$\eta_i^{TM} = \eta_0 \sqrt{\frac{\mu_i}{\varepsilon_i}} \cos\vartheta_i \tag{6}$$

$$\eta_i^{TE} = \eta_0 \sqrt{\frac{\mu_i}{\varepsilon_i}} \frac{1}{\cos\vartheta_i} \tag{7}$$

where $\cos\vartheta_1$ and $\cos\vartheta_2$ are derived from $\sin\vartheta_1$ and $\sin\vartheta_2$ evaluated by means of the Snell's law as:

$$\sin\vartheta_1 = \frac{\gamma_2}{\gamma_1} \sin\vartheta_2 \tag{8}$$

$$\sin\vartheta_2 = \frac{\gamma_0}{\gamma_2} \sin\vartheta_0 \tag{9}$$

in which the propagation constants γ_0, γ_1 and γ_2 are given by:

$$\gamma_0 = j\frac{\omega}{c_0} \tag{10}$$

$$\gamma_1 = j\frac{\omega}{c_0} \sqrt{\mu_1 \varepsilon_1} \tag{11}$$

$$\gamma_2 = j\frac{\omega}{c_0} \sqrt{\mu_2 \varepsilon_2} \tag{12}$$

In order to minimize the reflection coefficient, the hyperbolic inner impedance at the front surface of the reflector layer should be close to the free space wave impedance. Therefore, the following matching condition should be satisfied:

$$Z_{in}^{TM(TE)} = \eta_0^{TM(TE)} \tag{13}$$

This equation cannot be resolved analytically, and several approaches were developed to minimize *R* of single- or multi-layer Salisbury screens.

Indeed, the design process is focused on the analytical expressions of the optimal thicknesses d_1* and d_2* for assumed values of d_2 and d_1 respectively, frequency f^* and incidence angle ϑ_0.

According to the matching Equation (13), the real- and imaginary- part of $Z_{in}^{TM(TE)}$ should be equal to $\eta_0^{TM(TE)}$ and zero, respectively. The obtained transcendental equations cannot be resolved literally to obtain the optimal thicknesses d_1* and d_2*. Thus, a simplified approach is needed.

In particular, the Equation (4) of $Z_{in}^{TM(TE)}$ and the matching Equation (13) are combined together and then resolved in terms of d_1* and d_2* for given d_2 and d_2 values.

After some developments, the following expressions are obtained:

$$\tanh\left(\gamma_1 \cos\vartheta_1 d_1^{TM(TE)}\right) = \Phi_1^{TM(TE)} \tag{14}$$

$$\tanh\left(\gamma_2 \cos\vartheta_2 d_2^{TM(TE)}\right) = \Phi_2^{TM(TE)} \tag{15}$$

in which:

$$\Phi_1^{TM(TE)} = \frac{\sqrt{\frac{\mu_2}{\varepsilon_2}}\Gamma_2^{TM(TE)}\tan h(\gamma_2 \cos \vartheta_2 d_2) - 1}{\sqrt{\frac{\mu_1 \varepsilon_2}{\mu_2 \varepsilon_1}}\Gamma_{12}^{TM(TE)}\tan h(\gamma_2 \cos \vartheta_2 d_2) - \sqrt{\frac{\mu_1}{\varepsilon_1}}\Gamma_1^{TM(TE)}} \tag{16}$$

$$\Phi_2^{TM(TE)} = \frac{\sqrt{\frac{\mu_1}{\varepsilon_1}}\Gamma_1^{TM(TE)}\tan h(\gamma_1 \cos \vartheta_1 d_1) - 1}{\sqrt{\frac{\mu_1 \varepsilon_2}{\mu_2 \varepsilon_1}}\Gamma_{12}^{TM(TE)}\tan h(\gamma_1 \cos \vartheta_1 d_1) - \sqrt{\frac{\mu_2}{\varepsilon_2}}\Gamma_2^{TM(TE)}} \tag{17}$$

with:

$$\Gamma_1^{TM} = \left(\Gamma_1^{TE}\right)^{-1} = \cos \vartheta_1 / \cos \vartheta_0 \tag{18}$$

$$\Gamma_2^{TM} = \left(\Gamma_2^{TE}\right)^{-1} = \cos \vartheta_2 / \cos \vartheta_0 \tag{19}$$

$$\Gamma_{12}^{TM} = \left(\Gamma_{12}^{TE}\right)^{-1} = \cos \vartheta_1 / \cos \vartheta_2 \tag{20}$$

Finally, applying the $(\tan h^{-1})$-function to Equation (14) and to Equation (15), the following analytical expressions of the optimal thicknesses are derived:

$$d_1^{*TM(TE)} = \left| \frac{1}{2\gamma_1} \ln\left(\frac{1 + \Phi_1^{TM(TE)}}{1 - \Phi_1^{TM(TE)}}\right) \right| \tag{21}$$

$$d_2^{*TM(TE)} = \left| \frac{1}{2\gamma_2} \ln\left(\frac{1 + \Phi_2^{TM(TE)}}{1 - \Phi_2^{TM(TE)}}\right) \right| \tag{22}$$

In case of normal incidence, the optimal thicknesses $d_i^* = d_i^{*TM} = d_i^{*TE}$, with $i = 1, 2$, assumes the following simple expression:

$$d_i^* = \left| \frac{1}{2\gamma_i} \ln\left(\frac{1 + \Phi_i}{1 - \Phi_i}\right) \right| \tag{23}$$

in which Φ_i is given by Equations (16) and (17) assuming $\Gamma_i = \Gamma_i^{TM} = \Gamma_i^{TE} = 1$.

It is worth noting that, due to the analytical definition of $(\tan h^{-1})$-function and to the periodicity of $(\tanh)$-function, Equations (21)–(23) permit to evaluate the optimal thicknesses $d_1^*(d_2)$ and $d_2^*(d_1)$ giving rise to the relative minimum value of the reflection coefficient.

4. Absorber Design and Performances

The high-frequency bands of 5G next generation technology of UK/Europe/China, Korea and USA are reported in Table 1. For each frequency band, the central frequency f_c is also indicated.

Table 1. 5G high frequency bands of some countries.

Frequency Band [GHz]	f_c [GHz]	Country
24.25–27.50	25.87	Europe/UK/China
26.50–29.50	28.00	Korea
27.50–28.35	27.92	USA
37.00–40.00	38.50	USA

The optimal design is carried out assuming the target frequencies equal to 26 GHz, 28 GHz, and 39 GHz, which are close to the central values f_c reported in Table 1.

Moreover, two different graphene-based composites are selected for the realization of the lossy layers. The first one has a GNP concentration equal to 2% wt. with respect to the total resin amount, the second one employs 4% wt. of GNPs. It is worthwhile to notice that

higher GNP amounts lead to technical difficulties, compromising the cost effectiveness and the quality of the resulting layer.

4.1. Composite Filled with 2% of GNPs

The optimal thicknesses d_1* and d_2* are computed as functions of the given thicknesses d_2 and d_1, respectively, using Equation (23) for the composite filled with 2% wt. of GNPs in the case of normal incidence.

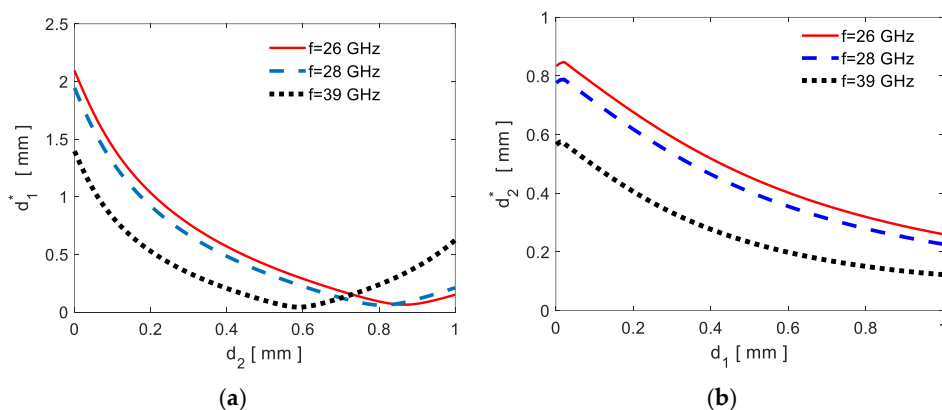The obtained results are represented in Figure 3.

(a)　　　　　　　　　　　　　　　　　　(b)

Figure 3. Optimal thickness d_1* as a function of d_2 (**a**) and optimal thickness d_2* as a function of d_1 (**b**), computed at the target frequencies of 26 GHz, 28 GHz and 39 GHz.

It should be noted that the same value of d_1* can be obtained considering two different values of d_2 in Figure 3a. The same discrepancy appears in Figure 3b for d_1 values lower than 0.5 mm. It yields that Equation (23) is not a one-to-one function, meaning that more thickness combinations can satisfy the matching condition.

In order to clarify and validate the proposed analytical approach, the reflection coefficient R is computed numerically by means of Equation (1) considering all the possible (d_1, d_2) combinations at the target frequencies. As an example, a 3D-map reporting the computed R values for d_1 ranging between 0 and 2.5 mm and d_2 between 0 and 1 mm at a frequency of 39 GHz is shown in Figure 4a. Successively, the d_1* value giving rise to the minimum reflection coefficient for each selected d_2 value is computed numerically. The obtained curve $d_1*(d_2)$ (red line) is reported in Figure 4b in which it also appears the curve computed by means of Equation (23) (black dotted line). It is worth noting that the curves are almost overlapping for d_2 values lower than 0.6 mm and the relative percent difference between them is always lower than 5% in the decreasing part of the $d_1*(d_2)$ curve.
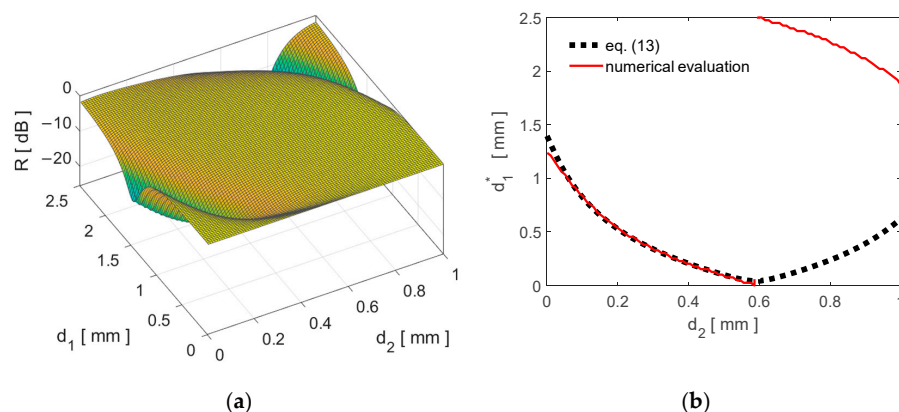

(a)　　　　　　　　　　　　　　　　　　(b)

Figure 4. 3D−map reporting the computed R values for all the (d_1, d_2) combinations in the selected d_1 and d_2 intervals at the target frequency of 39 GHz (**a**) and optimal thickness d_1* computed numerically (red line) or by Equation (13) (black dotted line) (**b**).

Figures 5–7 show the d_1* and d_2* values as functions of d_2 and d_1, respectively (blue dashed curves), while the red curves report the corresponding minimum R values for the assumed target frequencies.
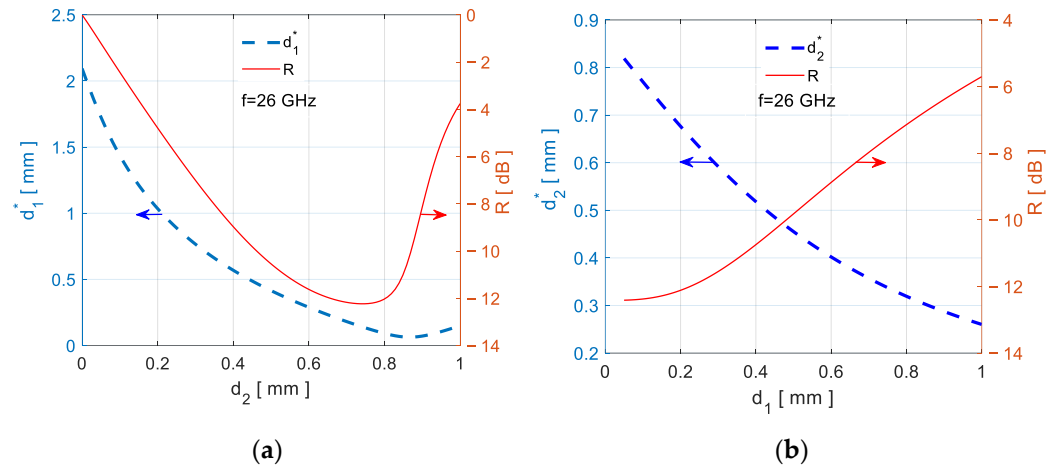

Figure 5. Optimal thicknesses $d_1*(d_2)$ (**a**) and $d_2*(d_1)$ (**b**) at target frequency of 26 GHz.
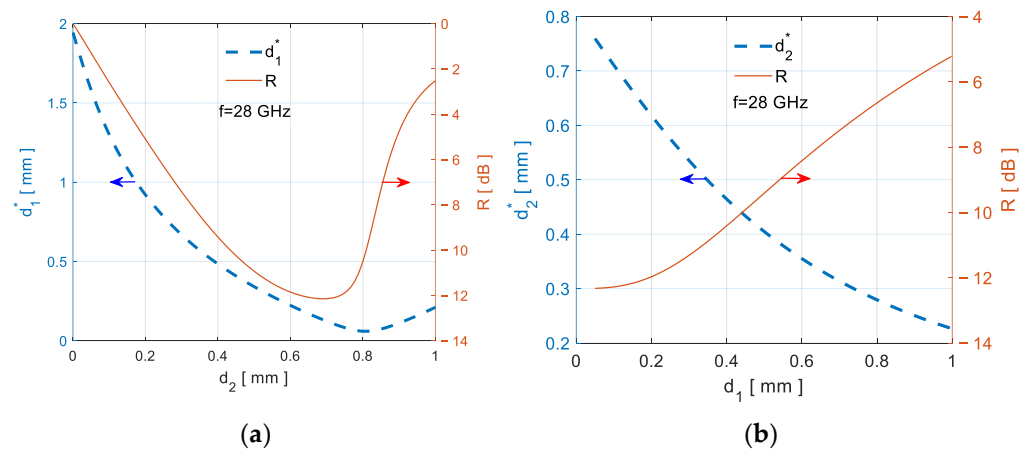

Figure 6. Optimal thickness $d_1*(d_2)$ (**a**) and $d_2*(d_1)$ (**b**) at target frequency 28 GHz.
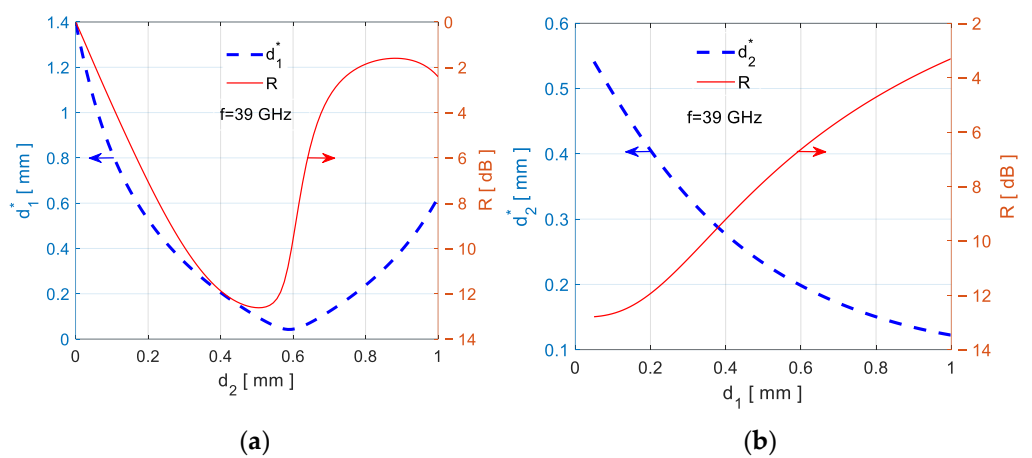

Figure 7. Optimal thicknesses $d_1*(d_2)$ (**a**) and $d_2*(d_1)$ (**b**) at target frequency of 39 GHz.

For instance, according to Figure 5a, obtained at the target frequency f = 26 GHz, assuming d_2, i.e., the thickness of the composite sheet, equal to 0.43 mm, the corresponding optimum spacer thickness d_1*= 0.5 mm should be selected in order to obtain the minimum

reflection coefficient $R = -11.2$ dB. Therefore, the lower minimum value $R^* = -12.1$ dB is obtained assuming $d_2 = 0.74$ and $d_1^* = 0.14$ mm. Similarly, from Figure 6a, obtained for $f = 28$ GHz, and Figure 7a, computed at $f = 39$ GHz, the lower values $R^* = -12.1$ dB and $R^* = -12.2$ dB can be achieved for $d_1^* = 0.12$ mm and $d_2 = 0.70$ mm or $d_1^* = 0.09$ mm and $d_2 = 0.5$ mm.

As expected, the same thickness values result from Figures 5b, 6b and 7b. Notice that when the optimal thickness values are selected in the increasing part of the curves representing d_1^* versus d_2 the reflection coefficient increases, resulting in a lower absorption performance. This fact confirms that only the decreasing part of the d_1^* versus d_2 curves should be considered.

Table 2 summarizes the obtained values of the lower minimum reflection coefficient R^* corresponding to the selected two-layers thicknesses at the target frequencies. These values are retrieved from Figures 5–7. In the same table, the corresponding bandwidths Δf at -10 dB are reported.

Table 2. Optimal thicknesses, lower minimum reflection coefficient and bandwidths at -10 dB for composite filled with 2% of GNPs at target frequencies in case of normal incidence.

Case	f^* [GHz]	R^* [dB]	d_1^* [mm]	d_2^* [mm]	Δf [GHz]
A	26	−12.1	0.14	0.74	24.0–27.6
B	28	−12.1	0.12	0.70	25.5–29.7
C	39	−12.2	0.09	0.50	36.2–43.0

It should be noted that the optimal thicknesses d_2^* of the composites reported in Table 2 may be of difficult realization or they may compromise the final absorbing structure flexibility. For this reason, different thicknesses may be preferred with consequent lower absorbing performances.

The real and imaginary parts of the two-layers input impedance given by Equation (3) should be theoretically close to η_0 and zero, respectively, according to the matching condition of Equation (8). This condition would be more easily satisfied in the case of pure conductive lossy sheets and dielectric spacers.

It should be noted that the GNP-filled composites considered in this work are characterized by conductive and dielectric properties, represented by the real and imaginary parts of the complex permittivity, as shown in Figure 2. As a consequence, the lossy sheet is not pure conductive, and the theoretical matching condition may not be fully satisfied. For instance, at the frequency of 26 GHz and assuming $d_1^* = 0.14$ mm and $d_2^* = 0.74$ mm it results Real(Z_{in}) = 546 Ω and Imag(Z_{in}) = -154 Ω, as shown in Figure 8a,b.
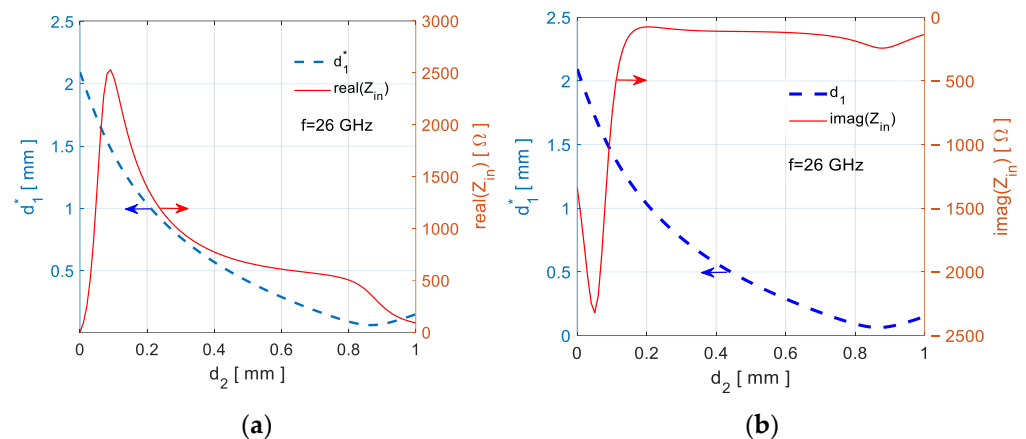

Figure 8. Real (**a**) and imaginary (**b**) parts of input impedance as function of $d_1^*(d_2)$ at a frequency of 26 GHz.

Finally, the reflection coefficient is computed in the 5G frequency band between 10 GHz and 40 GHz assuming the optimal thicknesses in Table 2. The obtained frequency spectra are represented in Figure 9. The minimum reflection coefficient R^* is obtained at the target frequencies of 26, 28, and 29 GHz, fulfilling the objectives of the optimal design.
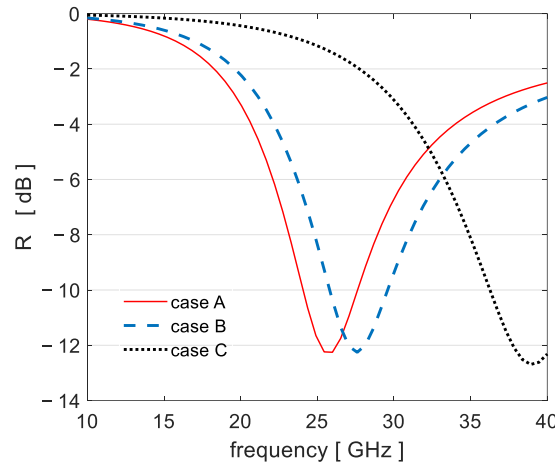

Figure 9. Frequency spectra of the reflection coefficient for the cases A, B and C shown in Table 2 for normal incidence.

4.2. Composite filled with 4% of GNPs

In order to improve the absorbing performance, the composite filled with 4% of GNPs is considered. Table 3 summarizes the obtained values of the lower minimum reflection coefficients R^* in case of normal incidence at the selected frequencies f^*, the optimum thicknesses d_1^* and d_2^* obtained following the procedure described in Section 3 and the corresponding bandwidths Δf at -10 dB.

Table 3. Optimal thicknesses, lower minimum reflection coefficient and bandwidths at -10 dB for composite filled with 4% of GNPs at target frequencies in case of normal incidence.

Case	f^* [GHz]	R^* [dB]	d_1^* [mm]	d_2^* [mm]	Δf [GHz]
A	26	-23.4	0.05	0.62	23.8–28.7
B	28	-23.0	0.05	0.58	25.4–30.8
C	39	-24.9	0.05	0.40	35.7–42.0

The obtained frequency spectra of the reflection coefficient for the cases A, B, and C in Table 3 are represented in Figure 10 for normal incidence.
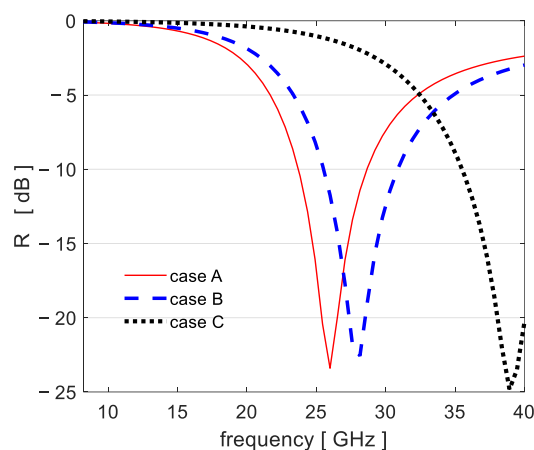

Figure 10. Frequency spectra of the reflection coefficient for the cases A–C shown in Table 3 for normal incidence.

Finally, the reflection coefficients R^{TM} and R^{TE} are computed for an incidence angle ranging between 0° and 30° and assuming the layer thicknesses reported in Tables 2 and 3 for the composite filled with 2% and 4% of GNPs, respectively. The obtained results are shown in Figures 11 and 12.
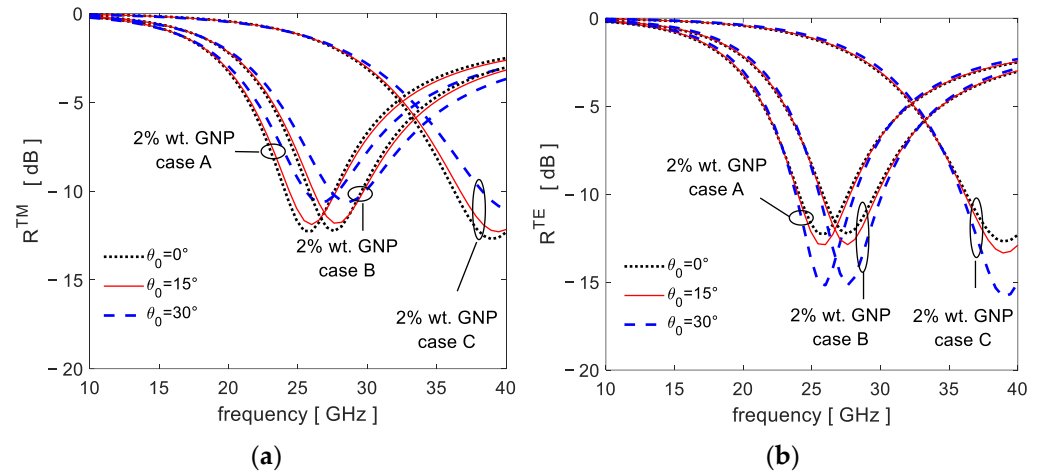
Figure 11. Reflection coefficients (**a**) R^{TM} and (**b**) R^{TE} as functions of the incidence angle for the cases A–C shown in Table 2 and composite filled with 2% of GNPs.
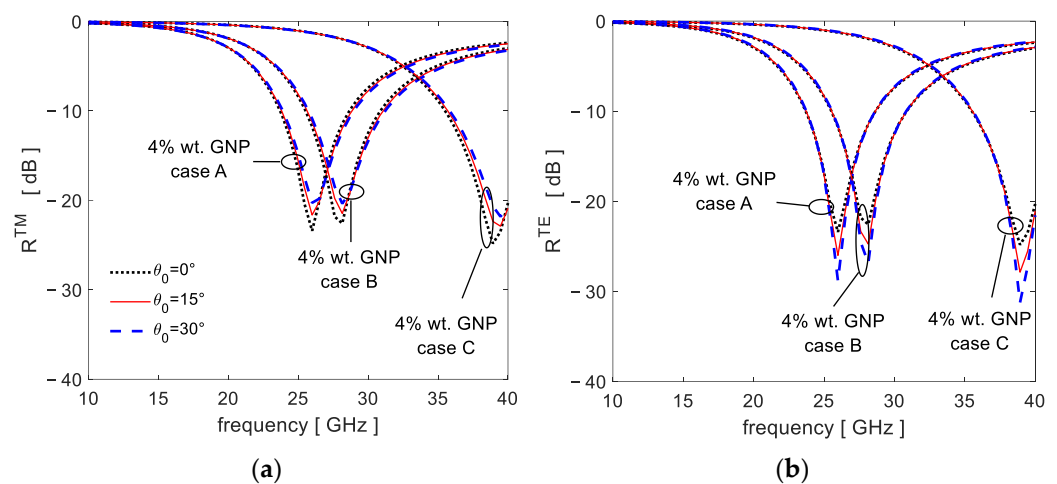
Figure 12. Reflection coefficients (**a**) R^{TM} and (**b**) R^{TE} as functions of the incidence angle for the cases A, B and C shown in Table 3 and composite filled with 4% of GNPs.

5. Conclusions

New analytical expressions to optimize the thicknesses of two-layers absorbers are derived applying the $(\tan h^{-1})$-function to the hyperbolic matching condition in case of oblique incidence of the impinging plane wave.

It should be noted that the design process only optimizes the spacer thickness if the lossy sheet thickness is selected or vice versa, avoiding time consuming numerical or iterative procedures. On the other hand, absorbing structures designed using complex algorithms, which are able to optimize both the two-layer thicknesses, can be not feasible or of difficult practical realization specially when graphene-based composites, characterized by both dielectric and conductive properties, are selected for the realization of the lossy layer.

The method is tested on absorbers consisting of an epoxy-based vinyl ester resin filled with 2% or 4% wt. of graphene nanoplatelets (GNPs) and a polypropylene dielectric spacer. Both the transverse magnetic (TM) and electric (TE) polarizations of the impinging plane waves are considered. The optimal thicknesses are computed at the target frequencies of

26, 28, and 39 GHz in order to obtain a −10 dB bandwidth able to cover the 5G frequency bands of Europe/UK/China, Korea, and USA between 23.8 and 40 GHz.

It should be noted that, due to the dielectric properties of the composites acting as lossy layers, the theoretical matching condition is not fully satisfied when the optimal thicknesses are considered.

The values of the optimal thickness of the spacer (or composite layer) as function of the selected thickness of the composite layer (or spacer) obtained applying the analytical approach in the case of normal incidence are validated by the comparison with the ones computed numerically considering all the possible combinations of the two-layers thicknesses.

The results obtained demonstrate the effectiveness and high accuracy of the proposed method, making it an ideal candidate for the development of an efficient design tool for absorber design optimization. This tool is of particular significance for this type of graphene based absorbing structure as it allows for the establishment of process parameters for the production of suitable GNP-filled composites, thereby reducing both production efforts and costs.

References

1. Thompson, J.; Ge, X.; Wu, H.C.; Irmer, R.; Jiang, H.; Fettweis, G.; Alamouti, S. 5G wireless communication systems: Prospects and challenges. *IEEE Commun. Mag.* **2014**, *52*, 62–64. [CrossRef]
2. Imoize, A.L.; Adedeji, O.; Tandiya, N.; Shetty, S. 6G enabled smart infrastructure for sustainable society: Opportunities, challenges, and research roadmap. *Sensors* **2021**, *21*, 1709. [CrossRef]
3. The Federal Communications Commission. New Rules Will Enable Rapid Development and Deployment of Next Generation 5G Technologies and Services. Washington. 14 July 2016. Available online: https://www.news4jax.com/tech/2016/07/15/new-fcc-rule-allows-for-next-generation-wireless-technology/ (accessed on 17 January 2023).
4. Ra'Di, Y.; Simovski, C.; Tretyakov, S. Thin perfect absorbers for electromagnetic waves: Theory, design, and realizations. *Phys. Rev. Appl.* **2015**, *3*, 037001. [CrossRef]
5. Jang, T.; Youn, S.; Shin, Y.; Guo, L. Transparent and flexible polarization-independent microwave broadband absorber. *Acs Photonics* **2014**, *1*, 279–284. [CrossRef]
6. D'Aloia, A.G.; D'Amore, M.; Sarto, M.S. Low-terahertz modeling of graphene/dielectric multilayers using an equivalent single layer in reverberation environment. *IEEE Trans. Electromagn. Compat.* **2017**, *60*, 849–857. [CrossRef]
7. Munk Ben, A. *Frequency Selective Surfaces: Theory and Design*; John Wiley & Sons: Hoboken, NJ, USA, 2005.
8. Mosallaei, H.; Rahmat-Samii, Y. RCS reduction of canonical targets using genetic algorithm synthesized RAM. *IEEE Trans. AP* **2000**, *48*, 1594–1606. [CrossRef]
9. Cui, S.; Weile, D.S. Application of a parallel particle swarm optimization scheme to the design of electromagnetic absorbers. *IEEE Trans. AP* **2005**, *53*, 3616–3624. [CrossRef]
10. Kim, J.-B.; Byun, J.-H. Salisbury screen absorbers of dielectric lossy sheets of carbon nanocomposite laminates. *IEEE Trans. EMC* **2012**, *1*, 37–42. [CrossRef]
11. He, Y.; Gong, R.; Nie, Y.; He, H.; Zhao, Z. Optimization of two-layer electromagnetic wave absorbers composed of magnetic and dielectric materials in gigahertz frequency band. *J. Appl. Phys.* **2005**, *98*, 084903. [CrossRef]
12. Zhang, H.; Zhao, Y.; Yang, X.; Zhao, G.; Zhang, D.; Huang, H.; Yang, S.; Wen, N.; Javid, M.; Fan, Z.; et al. Facile synthesis of novel amorphous TiO_2 nanorods decorated rGO hybrid composites with wide band microwave absorption. *Nanomaterials* **2020**, *10*, 2141. [CrossRef] [PubMed]
13. Liu, Y.; Liu, X.; Wang, X. Double layer microwave absorber based on CoFe2O4 ferrite and carbonyl iron composites. *J. Alloy. Compd.* **2014**, *584*, 249–253. [CrossRef]
14. Wei, C.; Shen, X.; Song, F.; Zhu, Y.; Wang, Y. Double layer microwave absorber based on nanocristalline $Zn_{0.5}Ni_{0.5}Fe_2O_4/\alpha$-Fe microfibers. *Mater. Des.* **2012**, *35*, 363–368. [CrossRef]
15. D'Aloia, A.; Marra, F.; Tamburrano, A.; De Bellis, G.; Sarto, M.S. Electromagnetic absorbing properties of graphene-polymer composite shields. *Carbon* **2014**, *73*, 175–184. [CrossRef]

16. Knott, E. The thickness criterion for single-layer radar absorbents. *IEEE Trans. AP* **1979**, *27*, 698–701. [CrossRef]
17. Rozanov, K.N.; Koledintseva, M.Y. Matching conditions for a homogeneous absorbing layer. *Procedia Eng.* **2017**, *216*, 79–84. [CrossRef]
18. D'Aloia, A.; D'Amore, M.; Sarto, M. Literal solutions for optimal design of microwave absorbing composites. In Proceedings of the 2021 IEEE International Joint EMC/SI/PI and EMC Europe Symposium, Raleigh, NC, USA, 26 July–20 August 2021.
19. D'Aloia, A.; D'Amore, M.; Sarto, M. Oblique incidence optimal design of microwave dielectric-magnetic absorbing composites. *IEEE Trans. Magn.* **2022**, *58*, 1–7. [CrossRef]
20. Pereira, P.; Ferreira, D.P.; Araújo, J.C.; Ferreira, A.; Fangueiro, R. The potential of graphene nanoplatelets in the development of smart and multifunctional ecocomposites. *Polymers* **2020**, *12*, 2189. [CrossRef] [PubMed]
21. Kamedulski, P.; Truszkowski, S.; Lukaszewicz, J.P. Highly effective methods of obtaining N-doped graphene by gamma irradiation. *Materials* **2020**, *13*, 4975. [CrossRef] [PubMed]
22. Jiménez-Suárez, A.; Prolongo, S.G. Graphene nanoplatelets. *Appl. Sci.* **2020**, *10*, 1753. [CrossRef]
23. Mittal, G.; Dhand, V.; Rhee, K.Y.; Park, S.J.; Lee, W.R. A review on carbon nanotubes and graphene as fillers in reinforced polymer nanocomposites. *J. Ind. Eng. Chem.* **2015**, *21*, 11–25. [CrossRef]
24. Bidsorkhi, H.C.; D'Aloia, A.G.; Tamburrano, A.; De Bellis, G.; Delfini, A.; Ballirano, P.; Sarto, M.S. 3D Porous graphene based aerogel for electromagnetic applications. *Sci. Rep.* **2019**, *9*, 1–11. [CrossRef] [PubMed]
25. D'Aloia, A.; Bidsorkhi, H.; Tamburrano, A.; Sarto, M. Graphene-based electromagnetic absorbing textiles for 5G frequency bands. In Proceedings of the 2022 IEEE International Symposium on Electromagnetic Compatibility & Signal/Power Integrity (EMCSI), Spokane, WA, USA, 1–5 August 2022.
26. Sarto, M.S.; D'Aloia, A.G.; Tamburrano, A.; De Bellis, G. Synthesis, modeling, and experimental characterization of graphite nanoplatelet-based composites for EMC applications. *IEEE Trans. Electromagn. Compat.* **2012**, *54*, 17–27. [CrossRef]